

Physico-chemical studies on raw and processed moth caterpillar silks from the mega-biodiversity hotspots of India

Pramod C. Mane¹, Nilam M. Qureshi², Manish D. Shinde², Sandesh R. Jadkar³, Dinesh P. Amalnerkar^{4,*} and Ravindra D. Chaudhari^{1,*}

¹Zoology Research Centre, Shri Shiv Chhatrapati College of Arts, Commerce and Science, Junnar, Pune 410 502, India

²Centre for Materials for Electronics Technology, Panchwati, Off Pashan Road, Pune 411 008, India

³School of Energy Studies, Department of Physics, Savitribai Phule Pune University, Pune 411 007, India

⁴School of Mechanical Engineering, Sungkyunkwan University, Suwon 440 746, South Korea

Silkworm fibre has been identified as a suitable material for biomedical and electronics applications because of its superior optical, mechanical and biological properties. Herein, we present comparative studies pertaining to the structural and morphological features of naturally harvested moth caterpillar silk fibre samples obtained from domesticated (*Bombyx mori*) as well as wild species, viz. *Antheraea mylitta* and *Antheraea papiha*. It has been observed that silk fibres obtained from silk cocoons are several microns in thickness. Surprisingly, wild variety, i.e. tasar silk samples show better structural and morphological properties. These fibres may find broad-spectrum applications in biomedical and electronics research.

Keyword: Degumming, mega-biodiversity hotspots, mulberry silk, silk cocoons, tasar silk.

BIOMATERIALS are gaining attention for various applications in diverse fields ranging from healthcare to bioelectronics. Natural fibres of plant and animal origin are one of the important links in the history of human evolution. Cotton and wool have received much attention in this context, while silk was popular among the rich. Natural silk is a macromolecule comprising polymeric protein in which the physical properties of fibroin bundles are controlled by different amino acids which leads to the production of, say, combinations of β -sheet (crystal-forming blocks) and amorphous (sometimes helical) structural regions^{1,2}. Such combinations of fibroin bundles form the backbone of fibres produced by silk worms or spiders. In the world of natural fibres, spider filament has been recognized as the wonder fibre for its unique combination of high strength and elongation at break. *Antheraea mylitta* and *Antheraea papiha* are economically important wild silk moth species distributed across India^{3,4}.

Silk, a natural polymer, is mainly produced by insects of families Bombycidae and Saturniidae. Silk obtained from domesticated silkworm *Bombyx mori* is known as mulberry silk and silk from all other sources is considered as non-mulberry silks⁵. Silks are produced by several insects. However, commercially, only the silk of moth caterpillars has been used in textile manufacturing as it contains a high proportion (50%) of glycine, which allows for tight packing making the fibres strong and resistant to breaking⁶. Their extraordinary tensile strength may be attributed to many interceded hydrogen bonds. When stretched, force is applied on these numerous bonds, but they do not break. Silk fibre extracted from *Bombyx mori*, is the most commonly used variety since ancient times. Silk fibres have more advantages like high strength, durability, lustre and other unique features compared to common cellulose and synthetic fibres. Since 1930, efforts have been made to produce protein fibres using various protein sources⁷.

Raw silk consists of two proteins – sericin and fibroin. The latter forms the structural centre of the fibre and the former forms the sticky material surrounding it. Fibroin is composed of the amino acids Gly–Ser–Gly–Ala–Gly–Ala and leads to formation of beta (β)-pleated sheets. The glue-like protein known as sericin carries out protective functions against microbial degradation, animal digestion and other damaging processes. Sericin also plays an important role in determining surface characteristic of the fibre. Silkworm fibre is valuable not only in textiles, but also in medical applications because of its superior mechanical properties and biocompatibility^{8,9}. Silk fibres are conventionally used for manufacturing surgical sutures. Silk fibroin has been used for non-textile applications, including biotechnology. It possesses some exceptional properties like non-toxicity, biocompatibility, and biodegradability and optical transparency in film form¹. Under all aqueous and mild processing conditions, enzymes and drugs can be incorporated into the silk matrix. Silk extracted from the wild as well as domestic caterpillar varieties can be used for various applications

*For correspondence. (e-mail: dpa54@yahoo.co.in; rdchaudhari2004@yahoo.co.in)

as a natural fibre and as extracted fibroin protein. For example, it is an attractive material for applications in biophotonics due to its biocompatibility, and unique mechanical and optical characteristics¹⁰⁻¹³. Additionally, silk films can be explored as a platform for bio-applications owing to numerous advances in micro and nanofabrication of such films. Recently, silk cocoon membranes have been shown to generate electrical current (either ionic or protonic origin) on absorbing moisture and have been explored for biosensor and humidity sensor applications¹⁴. Kundu *et al.*¹⁵ have published a review on non-mulberry silk biopolymers. However, they have not included the structural and morphological characterization of non-mulberry silk varieties¹⁵.

Understanding the structural, morphological and thermal properties of the pristine silks produced by caterpillar moths could be worthwhile to identify their unique aspects from the standpoint of scientific curiosity and prospective biotechnological applications. It may also be possible to develop recombinant or regenerated protein fibres from caterpillar silk moth for different applications. Studies on the physical and mechanical properties of such natural polymer composite materials will be of particular significance to achieve a deeper understanding of the evolution and physiology of silkworms, natural polymer processing system, and can presumably provide new insights into the biomimetic design of artificial structures¹⁶. It has been comprehended that the processed silk fibres and their derivatives can be exploited in silk sutures, drug delivery systems and fibre-based tissue products for ligament, bone and other tissue repairs as well as in the fabrication of sustainable, resorbable sensors and bio-integrated electronics^{13,17-19}.

In this context, we provide a comparative account of structural, thermal and morphological features of pristine as well as processed (degummed) silk fibres obtained from domesticated and wild moth species predominant in the northern Western Ghats (*Bombyx mori* and *Antheraea mylitta*) and Satpura range (*Antheraea papiha*), the mega-biodiversity hotspots of India. Interestingly, India is one of the 25 countries in the world possessing three mega-biodiversity hotspots. The Western Ghats and Satpura range are the cradles of biodiversity possessing thousands of varieties of flora and fauna, many of which are endemic to these regions. The Western Ghats is especially considered as one of the mega-biodiversity hotspots of the world owing to its prosperous biodiversity segment. For the present study, mulberry and tasar silk from the Western Ghats and Satpura range have been chosen. These fibres as biological template might suggest new directions to emulate in the pursuit of innovative high-performance, multifunctional materials generated with a green chemistry and processing approach. These bio-inspired and high-technology materials can lead to multifunctional material platforms that can integrate with living systems for medical materials and a

host of other applications like biosensing as envisioned^{13,17}.

Materials and methods

For studying the undegummed fibres, all the samples from different species were used as received. Two different silk varieties, namely silk from *Bombyx mori* and *Antheraea papiha* as well as *Antheraea mylitta* which are commonly known as mulberry and tasar silk respectively, have been used. However, two samples of tasar silk (sub-species), i.e. *Antheraea papiha* and *Antheraea mylitta* obtained from two different geographical locations, namely Western Ghats and Satpura range have been used. Silk fibre samples corresponding to undegummed mulberry and the two tasar silk samples from two different subspecies were labelled as UBM, UAP and UAM respectively. The silk cocoons were dried at 50°C in an oven and the loose threads were directly used. Multivoltine mulberry variety is reared by sericulturists in the selected geographical region and was used for the present study.

For degumming (removing of sericin coating), the silk cocoons were cut into smaller pieces and 5 g each of cut piece was boiled in 50 mM aqueous solution of sodium carbonate for 1 h. The fibres were then washed repeatedly in water three times and finally dried in a hot-air oven at 50°C overnight²⁰. Silk fibre samples corresponding to degummed mulberry and tasar from the northern Western Ghats and from Satpura range were labelled as DBM, DAP and DAM respectively.

X-ray diffraction (XRD) analysis of the undegummed and degummed samples was carried out using a diffractometer (Bruker AXS model D-8) equipped with a monochromator and Ni-filtered Cu-K α radiation ($\lambda = 1.54 \text{ \AA}$) with a scan speed of 4°/min. Thermal analysis of the samples was accomplished by thermogravimetric (TG) and differential scanning calorimetry (DSC) techniques (TA Instruments, USA; model no. SDTQ-600) at a heating rate of 10°C/min under N₂ atmosphere. For obtaining field emission scanning electron microscopic (FESEM) images (Hitachi S-4800, Japan), the fibre bundles were placed on a conducting carbon tape attached to an aluminium stub. These fibre bundles were coated with a thin layer of conducting gold film to minimize the effects due to charging. The Fourier transform infrared (FTIR) spectra (JASCO FTIR spectrophotometer) were recorded in the attenuated total reflection (ATR) mode for the degummed and undegummed fibres.

Results and discussion

X-ray diffraction

Figure 1 a and b shows the X-ray diffractograms corresponding to tasar and mulberry silk. Tasar silk revealed

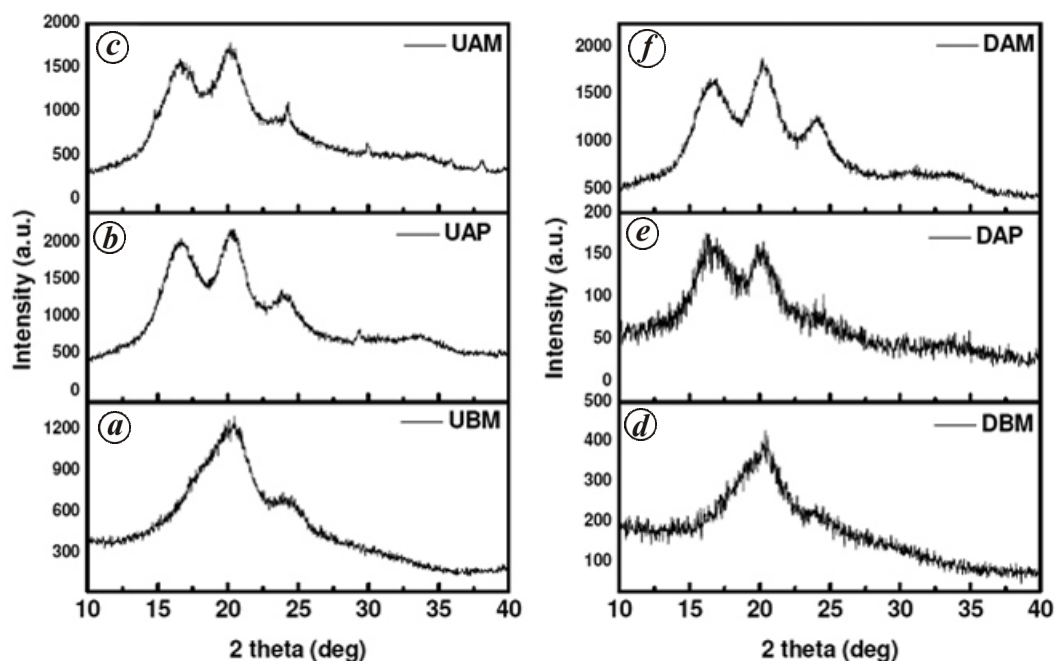


Figure 1. X-ray diffractograms corresponding to undegummed silk fibre samples: *a*, UBM; *b*, UAP; *c*, UAM; degummed silk fibre samples: *d*, DBM; *e*, DAP; *f*, DCH.

better crystallinity compared to mulberry silk. It is well known that *B. mori* silk fibroin can exist in two distinct structures in the solid state, namely silk-I and silk-II, which are conformations of β -sheet structures. The silk fibre produced by *A. mylitta* has its own distinctive colour, and is coarser than *B. mori* silk. However, tasar silk has higher tensile strength, elongation and stress-relaxation values than silk secreted by the domesticated silkworm *B. mori*. These properties have made tasar silk as desirable as *B. mori* silk for various applications like drug delivery, electronic appliances, sensors, etc.^{21–24}. In case of undegummed mulberry silk, a broad peak centred around 19.9° has been observed, which indicates predominance of silk-I crystalline nature for this sample (Figure 1 *a*). In case of undegummed tasar silk (Figure 1 *b* and *c*), the 2θ diffraction peaks correspond to the crystalline nature of silk-II ($2\theta = 16.3^\circ$ and 17.2°), and silk-I ($2\theta = 19.9^\circ$). A prominent diffraction peak at 2θ angle of 19.9° corresponds to (201) plane (d -spacing of 4.43 \AA)⁷. It has been reported that the amino acids glycine, alanine, serine and threonine constitute the crystalline regions in *B. mori* and common wild silks⁷. Peak broadening is a clear indication of nanocrystalline nature of these β -sheet structures. However, asymmetric behaviour of this peak on both sides indicates the presence of low-intensity peaks at 16.3° and 17.2° , which can be ascribed to the crystalline nature of silk-II. The broad hump centred around 22.31° also corresponds to the crystalline nature of silk-II for both tasar silk samples (UAP and UAM). After degumming, the structural behaviour akin to mulberry (Figure 1 *d*) as well as both the tasar silk fibres

(Figure 1 *e* and *f*) was observed. Nevertheless, all the samples displayed further peak broadening as well as reduction in the intensity of the peaks, which can be ascribed to the reduction in the crystallinity after the degumming that is an obvious feature in the processed samples. Interestingly, sharp yet low-intensity peaks at 24.35° , 29.90° , 35.86° and 38.04° have been observed for both the tasar silk samples before degumming. After degumming, only the peak at 24.35° was prominently noticed along with peak broadening, which may be due to significant reduction in particle size. These peaks can be indexed to the presence of α -calcium oxalate (CaC_2O_4) crystals (JCPDS 21-0838). It has been reported that calcium oxalate crystals co-exist with the wild varieties like tasar silk^{15,25}. The presence of calcium oxalate may help keep the tasar silk cocoon dry from the inside, even though it is found in the moisture-rich northern Western Ghats region. XRD results are consistent with those reported in the literature^{26,27}.

Thermogravimetry and differential scanning calorimetry

Figure 2 *a* shows TG curves of undegummed silk samples. The initial weight loss up to $\approx 80^\circ\text{C}$ observed for both the samples is due to loss of moisture. The second weight loss occurs in the range $225^\circ\text{--}375^\circ\text{C}$. This can be attributed to the breakdown of the side chain groups of the amino acid residues, as well as cleavage of the peptide bonds. It can be observed that mulberry silk shows 90%

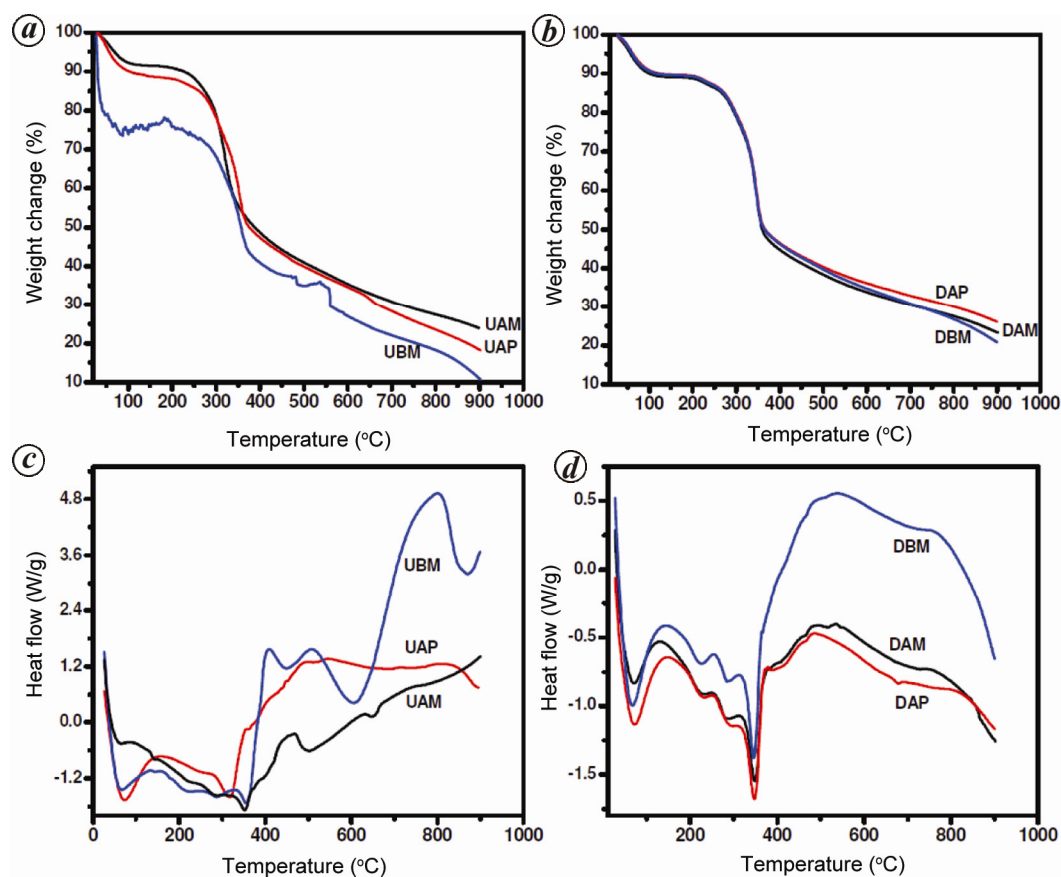


Figure 2. Thermal analysis of mulberry and tassar silk fibres using thermogravimetry: (a) before and (b) after degumming, and differential scanning calorimetry (c) before and (d) after degumming respectively.

degradation at 900°C. However, tassar silk samples show nearly 20–25% residues, which denotes their better stability at relatively higher temperature. Another important feature of tassar fibres is that they exhibit very low moisture loss (less than 10%) compared to mulberry fibres. This can be ascribed to the presence of calcium oxalate crystals in the tassar silk samples which keep them devoid of moisture. Figure 2b shows TG results of the samples after degumming.

All the three samples exhibit similar degradation behaviour which takes place in three steps, i.e. 10% weight loss due to moisture up to 100°C; 50% rapid weight loss up to 350°C and gradual weight loss till 900°C. However, all the samples retained 20–30% of the initial weight at 900°C, which can be ascribed to the slightly better thermal stability after degumming.

The procedural onset of the second degradation starts at 263°C, 261°C and 255°C for UBM, UAP and UAM samples respectively. After following a steep curve of weight loss up to 367°C, 360°C and 334°C, the respective weight loss to the tune of 30%, 31% and 28% has been noticed for UBM, UAP and UAM samples. This can be attributed to the breakdown of the side chain groups of the amino acids as well as cleavage of the peptide bonds. Subsequent to nearly 370°C, gradual weight loss is

observed till 900°C. However, in case of degummed silk samples (Figure 2b), all of them show more or less similar weight loss behaviour up to 350°C. The procedural onset of a weight loss begins at a lower temperature of nearly 225°C and ends at 350°C for all the samples. This lowering of onset may be attributed to the reduced crystallinity of the silk fibres after degumming. Surprisingly, 21%, 24% and 27% residue still persisted in the case of DBM, DAP and DAM samples respectively.

Figure 2c and d shows DSC results of the samples before and after degumming respectively. It is, however, interesting to note that such DSC graphs disclosing thermal changes in the samples down to 900°C have not been reported till date. The UBM sample shows first endotherm centred around 73°C, which can be attributed to loss of moisture (Figure 2c). A small endotherm is also noted at 244°C, which may be due to onset of second degradation. The second major endotherm is observed at 317°C, which may be due to breakdown of side chain and cleavage of peptide bonds. In case of UAP and UAM samples, the first endotherm is noted at 60°C which is not as broad as that for UBM sample (Figure 2d).

For these samples, the next endotherms are noted at 228°C and 289°C, which may be due to the second weight loss. The endotherm for the third weight loss is noticed

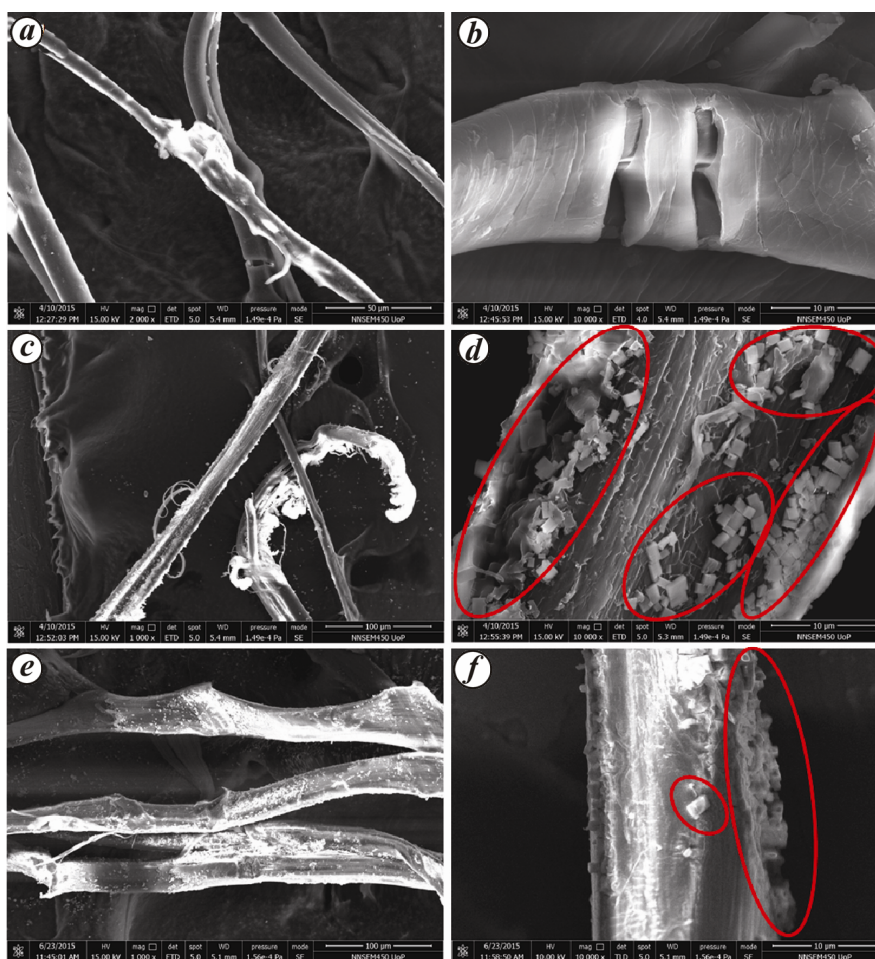


Figure 3. Field emission scanning electron microscopic (FESEM) images corresponding to undegummed silk fibre samples: (a, b) UBM, (c, d) UAP and (e, f) UAM at low (a, c and e) and high (b, d and f) magnification respectively.

to be shifted to higher temperature of 361°C and 352°C for UAP and UAM samples respectively. This endotherm is shifted by 35°C and 44°C for these samples compared to the UBM sample, which highlights their better thermal stability. For UAP sample, three more endotherms are observed at 453°C, 605°C and 863°C respectively, whereas two endotherms shifted at slightly higher temperatures of 494°C and 651°C are observed for the UAM sample. This result once again underlines the fact that the UAM sample possesses better thermal stability owing to better crystalline behaviour.

However, after degumming (Figure 2b), all the samples show similar behaviour. The first endotherm is observed at 69°C for DAM and DAP samples, and at 72°C for the DBM sample. This endotherm for the DMS sample is broader – similar to its undegummed counterpart. A decrease in temperature is noted for this sample, while an increase in temperature is found for the DAM and DAP samples. Nonetheless, their peaks have broadened, which may be ascribed to more moisture retention due to lack of calcium oxalate crystals in comparison to the undegummed counterparts. For all these samples, the

next endotherms are found out at 224°C, 287°C and 346°C. Thus, there is slight reduction in the degradation temperature for the second and third endotherms. It may be particularly noted that an endotherm at 289°C is not observed in case of UBM sample, but is found in DBM sample. Also, surprisingly, the endotherm at 317°C observed for the UBM sample has shifted to a higher temperature of 340°C for this sample. However, for other two samples, decrease in temperature of the endotherm by about 15°C and 7°C, compared to pristine samples reveals their reduced crystallinity and consequently lesser thermal stability. Unlike the undegummed samples, no significant endotherms have been observed above 400°C. These DSC results are stimulating but demand extensive data analysis, and efforts in this direction are underway.

Field emission scanning electron microscopy

Figure 3 shows FESEM images corresponding to the undegummed fibre samples. For undegummed sample image corresponding to mulberry silk, smooth surface is

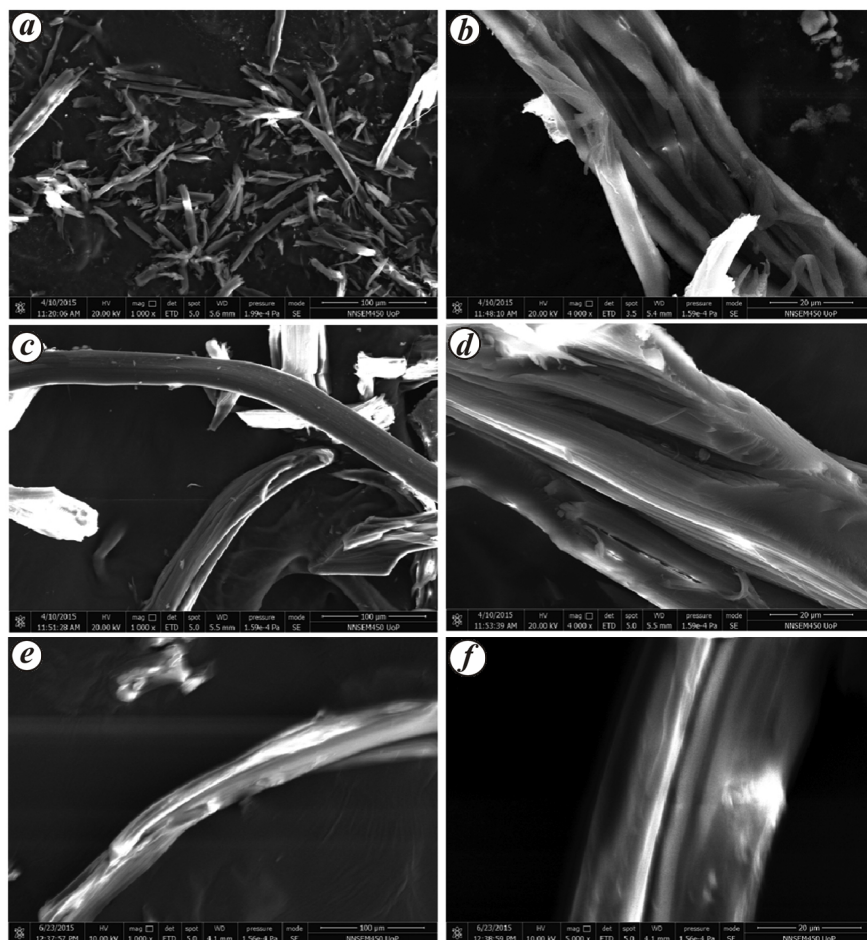


Figure 4. FESEM images corresponding to degummed silk fibre samples: (a, b) DBM, (c, d) DAP and (e, f) DAM at low (a, c and e) and high (b, d and f) magnification respectively.

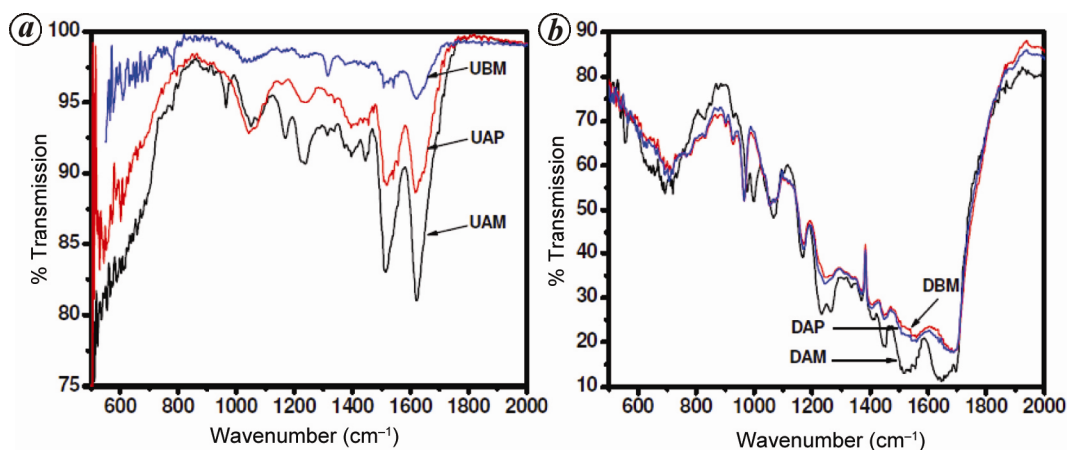


Figure 5. Fourier transform infrared spectra of silk samples: (a) undegummed and (b) degummed.

noticed. The thickness of the fibres is found to be 10–20 μm (Figure 3 a). Few cracks at certain places are also noticed. At higher magnification (Figure 3 b), the smooth surface is clearly observed. The presence of core and

sheath cable-like structure at the crack confirms that the outer sheath is made up of sericin and inner core is made up of fibroin. FESEM image for tasar silk sample corresponding to the Western Ghats region shows fibres with

relatively broader thickness distribution in the range of 10 to 40 μm (Figure 3 *c* and *d*). It also divulges the rough surface with the presence of numerous brick-like rectangular structures (marked with red circles in Figure 3 *d*).

The size of these structures varies from 1 to 5 μm . In case of tasar silk samples from Satpura range, samples with non-uniform thickness and rough surface have been identified (Figure 3 *e* and *f*). The thickness of the fibres varies from 40 to 80 μm . Similar to UAP samples, the prominent presence of brick-like structures over the surface of the fibres is detected (red circles in Figure 3 *f*). These brick-like structures are reported to be made up of calcium oxalate¹⁹. The calcium oxalate crystals not only provide rigidity to the cocoon, but also improve its barrier moisture management capacity.

Figure 4 shows FESEM images of the degummed silk fibre samples. After degumming, the DBM silk fibres have broken into smaller pieces (Figure 4 *a*). The thickness of the fibres has also decreased (5–10 μm). However, the fibres are found to coagulate with each other (Figure 4 *b*). The fibre surfaces are smooth. Additionally, core sheath-like structures are not noticed, which implies that sheath-forming sericin has been completely removed from the surface of the fibres.

In case of both tasar silk samples (Figure 4 *c–f*), fibre samples with smoother surfaces are found. The length of the fibres is more than the degummed mulberry silk samples. The brick-like calcium oxalate crystals are not observed.

Fourier transform infrared spectroscopy

FTIR spectra provide conformation information of different groups in an organic compound (Figure 5). Figure 5 *a* shows the FTIR spectra of undegummed silk fibres. The UAP sample shows sharper peaks with higher intensity which can be attributed to their better crystallinity. For the mulberry sample (UBM), the medium to strong peaks are noted at 780, 1311, 1508, 1542, 1618, 1646 cm^{-1} . Apart from these peaks, two broad humps centred around 1052 and 1221 cm^{-1} are observed. Very small peaks at 935, 962, 1159, 1377, 1446, 1456 and 1511 cm^{-1} have also been traced. These results substantiate amide I, amide II and amide III conformations with both the random coil and β -sheet behaviour. However, random coil nature seems to be predominant.

In case of UAP sample, strong and medium intensity peaks are observed at 1045, 1076, 1221, 1250, 1520, 1541, 1618 and 1646 cm^{-1} . Few low-intensity peaks are also observed at 797, 1156, 1308, 1339, 1394 and 1456 cm^{-1} . For the UAM sample, strong peaks are observed at 963, 1049, 1080, 1170, 1218, 1250, 1398, 1442, 1513, 1542, 1618 and 1643 cm^{-1} . Few low-intensity peaks are observed at 780, 796, 1313 and 1340 cm^{-1} . Compared to the UAP sample, the UAM sam-

ple exhibits sharper peaks with higher intensity, which indicates that the best crystalline behaviour can be seen in the UAM sample. An interesting situation arises after degumming, as the relative sharpness and intensity of the peaks for all the samples are drastically reduced (Figure 5 *b*). Both DBM and DAP samples demonstrate dominantly random coil behaviour. Even though DAM has retained predominantly β -sheet type of behaviour, peak broadening and reduction in peak intensity are indicative of increased significance of random coil behaviour.

For the DBM sample, major peaks were observed at 963, 1060, 1171, 1237 and 1656 cm^{-1} . Few low-intensity peaks were also located at 721, 924, 1238, 1408, 1449, 1511, 1539, 1560 and 1635 cm^{-1} . Almost identical peaks have been observed for the DAP sample. For the DAM sample, the peaks are relatively sharper. The major peaks are observed at 997, 1069, 1166, 1231, 1263 and 1446 cm^{-1} , and two very broad peaks centred at 1538 and 1638 cm^{-1} respectively, have also been observed. These two broad humps are made of peaks at 1512, 1535, 1556 cm^{-1} and 1618, 1635 and 1678 cm^{-1} respectively. These two humps are found to be reduced in intensity and increased in width compared to the undegummed counterparts of the same sample. There are few low-intensity peaks at 717, 831, 931, 1335, 1373 and 1408 cm^{-1} . From these FTIR spectra, it can be inferred that after degumming there is a reduction in the crystalline behaviour and improvement in the random coil (which is an indication of more amorphous nature) behaviour. These results are consistent with the XRD and TG–DSC results.

Conclusion

We have carried out a study on the physico-chemical properties of domestic and wild silk varieties before and after degumming. This study is particularly significant as it throws light on the properties of these silk varieties before and after degumming. Based on the insights gained, experiments for using degummed silk fibres as well as choice of type of silk fibre (wild or domestic) can be carried out keeping in mind the particular application domain.

1. Prasong, S., Wilaiwan, S. and Nualchai, K., Structure and thermal characteristics of *Bombyx mori* silk fibroin films: effect of different organic solvents. *Int. J. Chem. Technol.*, 2010, **2**, 21–27.
2. Steven, E. *et al.*, Physical characterization of functionalized spider silk: electronic and sensing properties. *Sci. Technol. Adv. Mater.*, 2011, **12**, 055002.
3. Raju, S. R., Manjeet, J. and Chidambaram, R., Studies on structure and properties of Nephila-spider silk dragline. *AUTEX Res. J.*, 2005, **5**, 30–39.
4. Chakraborty, S., Muthulakshmi, M., Vardhini, D., Jayaprakash, P., Nagaraju, J. and Arunkumar, K. P., Genetic analysis of Indian tasar silkmoth (*Antheraea mylitta*) populations. *Sci. Rep.*, 2015, **5**, 15728.

5. Dutta, S., Bharali, R., Devi, R. and Devi, D., Purification and characterization glue like sericin protein from a wild silkworm *Antheraea assamensis* Helfer. *Global J. BioSci. Biotechnol.*, 2012, **1**, 229.
6. Simmons, A. H., Michal, C. A. and Jelinski, L. W., Molecular orientation and two-component nature of the crystalline fraction of spider dragline silk. *Science*, 1996, **271**, 84–87.
7. Reddy, R. and Yang, Y., Structure and properties of cocoons and silk fibers produced by *Hyalophora cecropia*. *J. Mater. Sci.*, 2010, **45**, 4414–4421.
8. Osnat, H., David, P. K., Vollrath, F. and Vadgama, P., Spider and mulberry silkworm silks as compatible biomaterials. *Composites Part B: Eng.*, 2007, **38**, 324–337.
9. Mondal, M., Trivedy, K. and Kumar, S. N., The silk proteins, sericin and fibroin in silkworm, *Bombyx mori* Linn – a review. *Caspian J. Environ. Sci.*, 2007, **5**, 63–76.
10. Sunghwan, K., Alexander, N. M., Joshua, D. S., David, L. K. and Fiorenzo, G. O., Silk protein based hybrid photonic–plasmonic crystal. *Opt. Express*, 2013, **21**, 8897–8903.
11. Lawrence, B. D., Golomb, M. C., Georgakoudi, I., Kaplan, D. L. and Omenetto, F. G., Bioactive silk protein biomaterial systems for optical devices. *Biomacromolecules*, 2008, **9**, 1214–1220.
12. Amsden, J. J., Domachuk, P., Gopinath, A., White, R. D., Negro, L. D., Kaplan, D. L. and Omenetto, F. G., Rapid nanoimprinting of silk fibroin films for biophotonic applications. *Adv. Mater.*, 2010, **22**, 1746–1749.
13. Kim, D. H. *et al.*, Dissolvable films of silk fibroin for ultrathin conformal bio-integrated electronics. *Nature Mater.*, 2010, **9**, 511–517.
14. Tulachan, B. *et al.*, Electricity from the silk cocoon membrane. *Sci. Rep.*, 2014, **4**, 5434.
15. Kundu, S. C. *et al.*, Invited review non mulberry silk biopolymers. *Biopolymers*, 2012, **97**(6), 455–467.
16. Hong-ping, Z., Xi-Qiao, F., Shou-Wen, Y., Wei-Zheng, C. and Feng-Zhu, Z., Mechanical properties of silkworm cocoons. *Polymers*, 2005, **46**, 9192–9201.
17. Omenetto, F. G. and Kaplan, D. L., New opportunities for an ancient material. *Science*, 2010, **329**, 528–531.
18. MacLeod, J. and Rosei, F., Photonic crystals: sustainable sensors from silk. *Nature Mater.*, 2013, **12**, 98–100.
19. Taaa, H. *et al.*, Silk-based resorbable electronic devices for remotely controlled therapy and *in vivo* infection abatement. *Proc. Natl. Acad. Sci. USA*, 2014, **111**, 17385–17389.
20. Rockwood, D. N., Preda, R. C., Yucel, T., Wang, X., Lovett, M. L. and Kaplan, D. L., Materials fabrication from *Bombyx mori* fibroin. *Nat. Prot.*, 2011, **6**, 1612–1631.
21. Hiroyuki, S., Ken-ichi, O., Kozo, T., Yoko, T. and Hiromi, Y., X-ray structural study of noncrystalline regenerated *Bombyx mori* silk fibroin. *Int. J. Biol. Macromol.*, 2004, **34**, 259–265.
22. Hao, Z. *et al.*, Preparation and characterization of silk fibroin as a biomaterial with potential for drug delivery. *J. Transl. Med.*, 2012, **10**, 117.
23. Eden, S. *et al.*, Physical characterization of functionalized spider silk: electronic and sensing properties. *Sci. Technol. Adv. Mater.*, 2011, **12**, 055002(1–13).
24. Takayuki, A., Giuliano, F., Riccardo, I. and Masuhiro, T., Biodegradation of *Bombyx mori* silk fibroin fibers and films. *J. Appl. Polym. Sci.*, 2004, **91**, 2383–2390.
25. Roy, M. *et al.*, Carbondioxide gating in silk cocoon. *Biointerphases*, 2012, **7**, 1–4.
26. Asakura, T., Yamane, T., Nakazawa, Y., Kameda, T. and Ando, K., Structure of *Bombyx mori* silk fibroin before spinning in solid state studied with wide angle X-ray scattering and ¹³C cross-polarization/magic angle spinning NMR. *Biopolymers*, 2001, **58**, 521–525.
27. Dutta, S., Talukdar, B., Bharali, R., Rajkhowa, R. and Devi, D., Fabrication and characterization of biomaterial film from gland silk of muga and eri silkworms. *Biopolymers*, 2013, **99**, 326–333.

ACKNOWLEDGEMENTS. We thank Prof. T. R. N. Kutty (Indian Institute of Science, Bengaluru) for helpful discussions and ISRO–UoP Space Technology Cell, for funding the research project no. STC/1552. D.P.A. thanks the Ministry of Science, ICT and Planning (South Korea) for financial support through Brain Pool Program of KOFST.

Received 10 September 2016; revised accepted 22 March 2016

doi: 10.18520/cs/v113/i05/919-926